Stacking the Cosmic Web in fluorescent Ly α emission with MUSE

Sofia G. Gallego, Sebastiano Cantalupo, Simon Lilly, Raffaella Anna Marino, Gabriele Pezzulli, Joop Schaye, Lutz Wisotzki, Roland Bacon, Hanae Inami, Mohammad Akhlaghi, et al.

Monthly Notices
of the
ROYAL ASTRONOMICAL SOCIETY

MNRAS **475,** 3854–3869 (2018)
Advance Access publication 2018 January 9

doi:10.1093/mnras/sty037

Stacking the Cosmic Web in fluorescent Ly α emission with MUSE

Sofia G. Gallego,[1]★ Sebastiano Cantalupo,[1]★ Simon Lilly,[1]★ Raffaella Anna Marino,[1] Gabriele Pezzulli,[1] Joop Schaye,[2] Lutz Wisotzki,[3] Roland Bacon,[4] Hanae Inami,[4] Mohammad Akhlaghi,[4] Sandro Tacchella,[1] Johan Richard,[4] Nicolas F. Bouche,[5] Matthias Steinmetz[3] and Marcella Carollo[1]

[1]*Department of Physics, ETH Zürich, CH-8093 Zürich, Switzerland*
[2]*Leiden Observatory, Leiden University, PO Box 9513, NL-2300 RA Leiden, the Netherlands*
[3]*Leibniz-Institut für Astrophysik Potsdam, AIP, An der Sternwarte 16, D-14482 Potsdam, Germany*
[4]*Univ Lyon, Univ Lyon1, Ens de Lyon, CNRS, Centre de Recherche Astrophysique de Lyon UMR5574, F-69230 Saint-Genis-Laval, France*
[5]*CNRS/IRAP, 9 Avenue Colonel Roche, F-31400 Toulouse, France*

Accepted 2018 January 3. Received 2017 December 19; in original form 2017 June 12

ABSTRACT

Cosmological simulations suggest that most of the matter in the Universe is distributed along filaments connecting galaxies. Illuminated by the cosmic UV background (UVB), these structures are expected to glow in fluorescent Ly α emission with a surface brightness (SB) that is well below current limits for individual detections. Here, we perform a stacking analysis of the deepest MUSE/VLT data using three-dimensional regions (subcubes) with orientations determined by the position of neighbouring Ly α galaxies at $3 < z < 4$. Our method increase the probability of detecting filamentary Ly α emission, provided that these structures are Lyman-limit systems (LLSs). By stacking 390 oriented subcubes we reach a 2σ sensitivity level of SB $\approx 0.44 \times 10^{-20}$ erg s^{-1} cm^{-2} arcsec^{-2} in an aperture of 1 arcsec^2 $\times$ 6.25 Å, three times below the expected fluorescent Ly α signal from the Haardt & Madau UVB at $z \sim 3.5$. No detectable emission is found on intergalactic scales, implying that at least two thirds of our subcubes do not contain oriented LLSs. On the other hand, significant emission is detected in the circumgalactic medium (CGM) in the direction of the neighbours. The signal is stronger for galaxies with a larger number of neighbours and appears to be independent of any other galaxy properties. We estimate that preferentially oriented satellite galaxies cannot contribute significantly to this signal, suggesting instead that gas densities in the CGM are typically larger in the direction of neighbouring galaxies on cosmological scales.

Key words: intergalactic medium – large-scale structure of universe.

1 INTRODUCTION

Our standard cosmological paradigm predicts that structures in the Universe grew from initial Gaussian quantum fluctuations into a 'Cosmic Web' of intergalactic filaments (e.g. Peebles & Groth 1975; Bond, Kofman & Pogosyan 1996) where galaxies form and evolve. However, most of the baryonic material in these filaments is expected to be too diffuse to form stars.

In the local universe, it has been empirically demonstrated that the large-scale distribution of galaxies and the velocity field are consistent with the predicted filamentary structure (see e.g. Libeskind et al. 2015). At high redshift, the first evidence of an intergalactic medium (IGM) came from the analysis of absorption lines in the spectra of quasars (see Rauch 1998 for a review). Unfortunately, given the one-dimensional nature of these absorption probes we have still little direct information on the spatial distribution and small-scale properties of intergalactic gas. Direct imaging of the Cosmic Web is in principle possible through fluorescent Ly α emission (Hogan & Weymann 1987; Gould & Weinberg 1996; Haiman & Rees 2001; Cantalupo et al. 2005). In particular, it is expected that gaseous filaments illuminated by ionizing radiation from the cosmic UV background (UVB) or local sources should emit Ly α radiation following hydrogen recombinations. For self-shielded gas clouds, about 60 per cent of the incident ionizing radiation should be converted to fluorescent Ly α emission (Gould & Weinberg 1996, but see Cantalupo et al. 2005). Such clouds therefore act as a kind of mirror of the UVB if they are away from bright UV sources such as quasars. In the spectra of a quasar,

★ E-mail: gallegos@phys.ethz.ch (SGG); cantalupo@phys.ethz.ch (SC); simon.lilly@phys.ethz.ch (SL)

self-shielded clouds correspond to Lyman-limit systems (LLSs; with column densities of neutral hydrogen $N_{\rm H\,I} > 10^{17.2}\,{\rm cm}^{-2}$) and Damped Ly α systems (DLA; with $N_{\rm H\,I} > 10^{20.3}\,{\rm cm}^{-2}$) although the latter are typically much rarer (Peroux et al. 2003; Prochaska, O'Meara & Worseck 2010; Noterdaeme et al. 2014). Ly α imaging of the typical LLSs should then provide direct constraints on the value of the cosmic UVB.

Previous attempts to detect fluorescent Ly α emission induced by the cosmic UVB have been unsuccessful. The deepest spectroscopic observation (a 92 h exposure with the VLT/FORS2 instrument) conducted so far reached a 1σ surface brightness (SB) limit of 8×10^{-20} erg s^{-1} cm^{-2} arcsec^{-2} per arcsec^2 aperture at $z \approx 3$ (Rauch et al. 2008). This observation used a long slit probing a total area of 2 arcsec $\times$ 453 arcsec ($\approx$0.25 arcmin^2) and a redshift range of $2.67 < z < 3.75$. Given the large redshift range probed and the observed incident rate of LLSs of about 1.5 per unit redshift at $z \approx 3$, (e.g. Prochaska et al. 2010), a large number of fluorescently emitting LLSs could have been detected in this study. This null result implied an upper limit on the UVB ionization rate of $\Gamma_{\rm H\,I} < 2.7 \times 10^{-12}\,{\rm s}^{-1}$ at 1σ at $z \approx 3$.

What are other observational and theoretical constraints on the cosmic UVB? Using the so-called proximity effect, i.e. the decrease in the number density of Ly α forest lines in proximity of quasars due to the increased ionizing radiation, we can put limits on the average intensity of the UVB at the Lyman-limit, e.g. $J = (9 \pm 4) \times 10^{-22}$ erg cm^{-2} s^{-1} Hz^{-1} sr^{-1} (Dall'Aglio, Wisotzki & Worseck 2008; see also, e.g. Carswell et al. 1987; Bajtlik, Duncan & Ostriker 1988; Scott et al. 2000; Calverley et al. 2011). These measurements, however, may be affected by clustering in the proximity of quasars or errors in the estimates of the quasars' ionizing luminosities and systemic redshifts. An alternative method uses the mean flux in the Ly α forest in combination with numerical simulations where the UVB is adjusted until the mean flux in artificial Ly α forest spectra matches the real data (see e.g. Rauch et al. 1997; Bolton et al. 2005; Faucher-Giguère et al. 2008; Becker & Bolton 2013). This method typically gives systematically lower values (by about a factor of 2–3, depending on the UVB spectral energy distribution) for the amplitude of the UVB compared to the proximity-effect measurements, although different works in the literature have discrepancies of a factor up to 2 due to different IGM temperatures in the simulations (see e.g. Becker & Bolton 2013 for a discussion).

Overall, these studies suggest that the UVB hydrogen ionization rate should be around $0.8 \times 10^{-12}\,{\rm s}^{-1}$ at $z \approx 3.5$ with very little evolution in the redshift range $2.5 < z < 4.5$ (e.g. Becker & Bolton 2013). Predictions made with synthesis UVB models, e.g. Haardt & Madau (1996), Faucher-Giguère et al. (2009), Haardt & Madau (2012, hereafter HM12), produce similar values of $\Gamma_{\rm H\,I}$ but suggest a more pronounced redshift evolution, mostly due to the assumed fraction of photons from galaxies and from the extrapolation of the observed quasar luminosity functions to the faint-end. In particular, the models from HM12 predict $\Gamma_{\rm H\,I} \approx 0.95 \times 10^{-12}\,{\rm s}^{-1}$ at $z = 2.5$ and lower by a factor of 1.7 at $z = 4$.

Given these low values of $\Gamma_{\rm H\,I}$, it is clear that the expected fluorescent emission from the UVB is out of reach for current facilities. Indeed, the expected UVB fluorescence SB for $\Gamma_{\rm H\,I} = 0.7 \times 10^{-12}\,{\rm s}^{-1}$ is 1.14×10^{-20} erg s^{-1} cm^{-2} arcsec^{-2} at redshift $z = 3.5$ (see e.g. Cantalupo et al. 2005), whereas with the new MUSE integral-field spectrograph the achieved 2σ SB limit is $\sim 10^{-19}$ erg s^{-1} cm^{-2} arcsec^{-2} at 5500 Å for an apperture of 1 arcsec^2 in a 30 h data cube (Bacon et al. 2017). One way to detect fluorescent Ly α emission above current observational limits is to look in the vicinity of bright quasars whose radiation can enhance the incident radiation by several orders of magnitude (Cantalupo et al. 2005; Kollmeier et al. 2010). In recent years, quasar-induced fluorescent emission has been detected by means of specifically designed narrow-band (NB) filters and with MUSE (see Cantalupo, Lilly & Haehnelt 2012; Cantalupo et al. 2014; Hennawi et al. 2015; Arrigoni Battaia et al. 2016; Borisova et al. 2016 and Cantalupo 2017 for a review). In addition to providing a new observational window on the circumgalactic medium (CGM) of galaxies hosting quasars, these observations can constrain the quasar emission properties. However, they do not give us any constraints on the cosmic UVB.

Without the boosting effect of quasars there are no alternatives for the detection of fluorescent emission from the UVB with current facilities other than stacking a series of deep observations. Typical Ly α stacking methods used so far in the literature assume a circularly symmetric distribution of emission (e.g. Steidel et al. 2011; Xue et al. 2017). Cosmological simulations suggest instead that the gas distribution between galaxies should be filamentary and that the filaments should be oriented preferentially towards neighbouring galaxies (e.g. Bond et al. 1996; Gheller et al. 2015).

In this study, we develop and apply the idea of an 'oriented stacking' approach[1] using Ly α emitting galaxies (LAEs) detected in deep MUSE cubes as reference points for the three-dimensional orientation of each stacking element. If neighbouring galaxies are indeed connected by (straight) filaments and if these filaments contain LLSs, then our oriented-stacking method should boost the signal-to-noise ratio (SNR) of UVB-induced fluorescence in IGM filaments by about the square root of the number of stacking elements. As we show in this paper, by using the deepest MUSE data cubes currently available and by staking more than 300 individual, 're-oriented subcubes around galaxies we are able to achieve a nominal 3σ detection limit of SB $\approx 0.78 \times 10^{-20}$ erg s^{-1} cm^{-2} arcsec^{-2} in an aperture of 0.4 arcsec^2 for a pseudo-NB of width 6.25 Å, well below the expected fluorescent signal from the values of the cosmic UVB reported above. In case of a positive detection, this method could also provide direct information on the size and distribution of LLSs and intergalactic filaments in emission away from quasars, thus giving us constraints on the size and morphological properties of these systems.

The paper is organized as follows. In Section 2 we describe the data and the selected galaxy catalogue. Section 3 describes the stacking procedure, sample selection and coordinate transformations. Results and discussion are shown in Sections 4 and 5, respectively and a summary is presented in Section 6. Throughout the paper we assume a flat ΛCDM cosmology with $H_0 = 69.6\,{\rm km\,s^{-1}\,Mpc^{-1}}$, $\Omega_{\rm m} = 0.286$ and $\Omega_\Lambda = 0.714$ (Bennett et al. 2014).

2 THE DATA

MUSE is a second generation instrument mounted on the Very Large Telescope (VLT) at the Paranal Observatory, Chile, and part of the European Southern Observatory (ESO). It is a panoramic integral-field spectrograph with a field of view (FOV) of 1 arcmin $\times$ 1 arcmin and a wavelength range of 470 nm $< \lambda <$ 940 nm (Bacon et al. 2010) with a spatial and wavelength sampling of 0.2 arcsec $\times$ 0.2 arcsec and 1.25 Å, respectively. To date, two very deep integrations (total exposure time per field of about 27–31 h) have been obtained during commissioning and as a part of the MUSE Guaranteed Time of

[1] We notice that a similar idea was also proposed in van de Voort & Schaye (2013), however a quantitative analysis was not presented in that study.

Observations (GTO): the Hubble Deep Field South (HDFS) (Bacon et al. 2010) and the MUSE Ultra Deep Field (UDF) (Bacon et al. 2017). The HDFS observation was obtained during the last commissioning run of MUSE with a 27 h exposure time in a field of 1 arcmin^2. The UDF observations consist of a mosaic of nine 10 h exposure fields obtained during GTO of the MUSE Consortium, plus an overlapping 31 h exposure in a 1.15 arcmin^2 field.

For the HDFS we use an improved data reduction obtained with the CubExtractor package (Cantalupo, in preparation; see also Borisova et al. 2016 for a short description) that will be presented in a separate paper. The full data reduction of the UDF field is described in Bacon et al. (2017) (see also Conseil et al. 2016). In this paper we use both the HDFS field and the deepest part of the UDF observation, called UDF-10 (hereafter UDF), which have similar depths.

The catalogue of LAEs in the HDFS was extracted from Bacon et al. (2015) and contains 89 LAEs including 26 LAEs not detected in the HST WFPC2 deep broad-band images. For the UDF, we use a preliminary LAE catalogue (Inami et al. 2017), that, combined with the HDFS catalogue, gives us a total of 247 LAEs.

During the stacking procedure, the images were centred in the 3D peaks of the Ly α emission that we have re-estimated with respect to the original catalogues. Finally, we discard LAEs with low confidence levels (e.g. objects with low signal-to-noise or possible interlopers) and sources closer than 2 arcsec to the edge. When pairs of LAE (i.e. objects within 3 arcsec from each other) are present in the catalogue, we discard the faintest of the two. Applying these criteria we discarded 36 LAEs from the initial catalogues.

3 STACKING PROCEDURE

In this section we explain how we obtained a set of oriented subcubes around galaxies in the direction of their neighbours for the stacking procedure. As discussed in Section 1, if galaxies are connected by filaments with column densities equal to or higher than those of LLSs, our stacking analysis should significantly enhance the expected fluorescent Ly α signal.

3.1 Sample selection

As a first criterion for our stacking procedure we select a set of galaxy neighbours within line-of-sight comoving distances (π) between 0.5 and 20 Mpc (cMpc) (Fig. 1, lower panel). Our choice of the distance upper limit is driven by the need of a large sample of galaxies to reach the required fluorescent emission levels (discussed in Section 1). However, we limit this distance to 20 cMpc because we expect that the probability that two galaxies are connected by a filament should rapidly decrease with galaxy distance (see e.g. Gheller et al. 2015, fig. 8). We find that 20 cMpc is the best compromise between these two factors. Because we are mostly interested in intergalactic scales and because of uncertainties due to peculiar velocities, we limit the smaller distances to 0.5 cMpc.

We select the redshift range of $2.9 < z < 4$ where $z = 2.9$ is the minimum Ly α redshift covered by MUSE and we restrict the range to $z < 4$ to minimize cosmological SB redshift-dimming effect.

Moreover, we discard neighbours closer than 16 arcsec in the plane of the sky (Fig. 1, upper panel) to avoid confusion between the Ly α emission coming from the galaxies or their CGM and the potential filamentary structure. We did not use a larger projected distance limit to avoid reducing too much the number of subcubes available for the stacking analysis. Within this particular distance range a single LAE can have up to 15 neighbours.

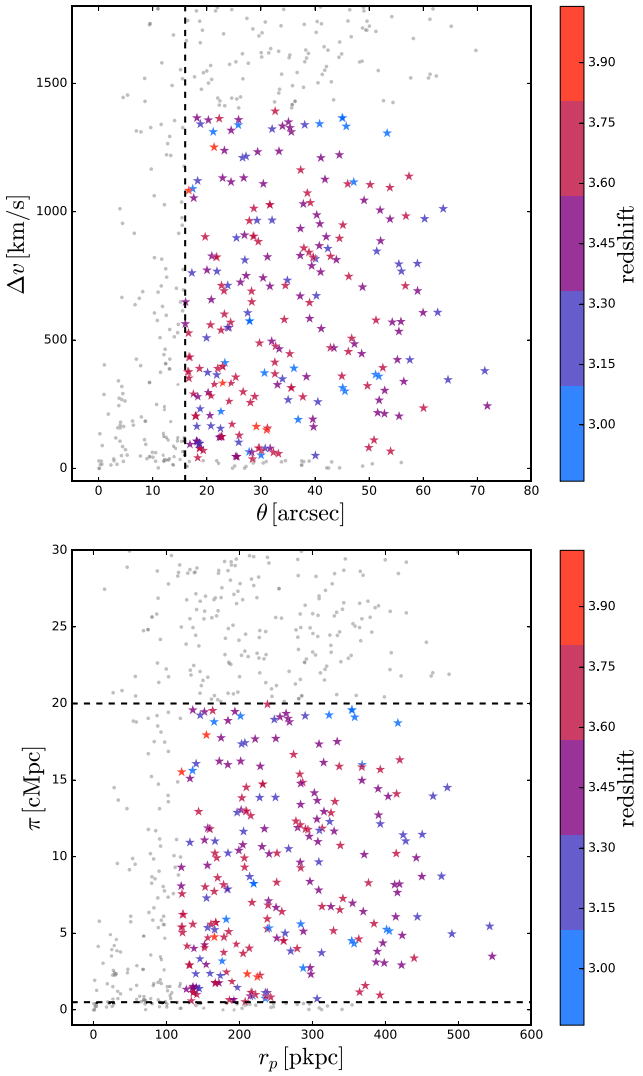

Figure 1. Projected (θ and r_p) versus line-of-sight (Δv and π) distribution of LAE neighbours, colour coded by their average redshift. The top panel presents the observationally derived quantities while the bottom panel shows the inferred values given our chosen cosmological parameters (projected coordinates are in physical kpc whereas line of sight coordinates in comoving Mpc). The dashed lines represent our selection criteria in both projected and line-of-sight distances. Notice that our projected distance range is much smaller than the line-of-sight separations because of the limited MUSE field of view (1 arcmin × 1 arcmin). Therefore, any neighbours at distances larger than 600 kpc in projected space will not be present in our catalogue. Grey points represent neighbours outside our selection criteria. These plots are similar but not identical because of the large range of redshifts.

The final sample consists of a set of 96 LAEs and 195 LAE neighbours, or equivalently 2 × 195 orientations. This corresponds to a cumulative exposure time of ∼10 000 h.

3.2 Subcubes transformation and stacking

For each individual LAE in our sample we select a region – centred on the LAE – with spatial size of 32 arcsec × 32 arcsec and wavelength width of 12.5 Å that has been re-oriented with respect to the original data cube applying the coordinate transformation described below.

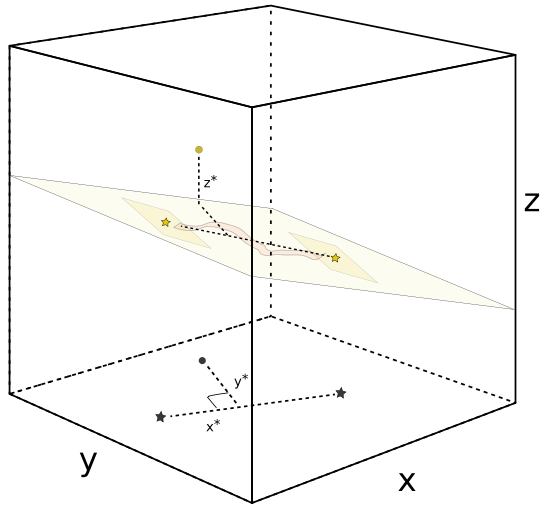

Figure 2. Cartoon representation of the subcube coordinate transformation (see the text for details). The yellow stars represent the positions of the LAEs in the cube and the pink region depicts a possible filament. The yellow point indicates the position of a particular voxel in the cube. The same objects in projected coordinates are represented in black. The light-yellow layer containing the two LAE positions represents the plane for which the transformed z coordinate (z^*) is equal to zero, whereas the yellow regions around each LAE represent the central layer of the extracted and transformed subcubes with a spatial size of 32 arcsec × 32 arcsec.

Before coordinate transformation, we performed continuum subtraction using a median filter approach as in Borisova et al. (2016) and masking continuum sources to avoid any continuum flux contamination. Moreover, we masked a small fraction of wavelength layers in correspondence of bright sky-lines to avoid being contaminated by skyline residuals.

Then, we apply a 2D transformation of the spatial coordinates in such a way that the resulting angle between the LAE and its neighbour is always zero with respect to the x-axis of the transformed coordinates. This means that for each voxel in the cube with coordinates $\boldsymbol{c} = (x, y)$ (independent of z) there will be a new set of coordinates $\boldsymbol{c}^* = (x^*, y^*)$ defined by

$$x^* = \frac{\boldsymbol{u} \,.\, \boldsymbol{d}}{|\boldsymbol{d}|}, \quad y^* = \frac{|\boldsymbol{u} \times \boldsymbol{d}|}{|\boldsymbol{d}|}, \tag{1}$$

where $\boldsymbol{d} = \boldsymbol{c}_n - \boldsymbol{c}_l$ is the projected distance between the LAEs, $\boldsymbol{c}_l$ and $\boldsymbol{c}_n$ are the spatial coordinates of the galaxy and its neighbour, respectively, and $\boldsymbol{u} = \boldsymbol{c} - \boldsymbol{c}_l$.

The third coordinate is derived by *shearing* the z coordinate (λ) with respect to the LAEs as

$$z^* = z - z_l - \frac{(z_n - z_l)\, x^*}{|\boldsymbol{d}|}\,. \tag{2}$$

The use of the shear is driven by the necessity of accounting for the maximum possible emission of the filament along the direction of the neighbour, by assuming that the wavelength is equivalent to a distance (therefore omitting any effect of peculiar velocities) and that the filaments are in a straight line between the galaxies. By using this method we also preserve the spectral shape of the Ly α emission coming from the LAEs and their surroundings. Among our sample, the shear is normally distributed around zero with a standard deviation of 10 pixels. In these coordinates $(0, 0, 0)$ and $(|\boldsymbol{d}|, 0, 0)$ are the new positions of the LAE and its neighbour, respectively. Fig. 2 shows a cartoon representation of the coordinate transformation procedure in the cube for a given combination of LAEs.

With this approach, LAEs close to the border will not have available data on some part of the subcube outside of our region of interest (i.e. the transformed voxels on the positive part of the x-axis). In this case, we fill the missing values with NaNs.

The new x^* and y^* coordinates are resampled with a bin size twice as large as the original one to avoid empty voxels, whereas the wavelength coordinate z^* is preserved. The spatial sampling of the transformed subcubes is therefore 0.4 arcsec × 0.4 arcsec. The voxel value (omitting NaNs) is assigned to the nearest new voxel to conserve the flux with respect to the initial cube.

As a consequence of the resampling method plus the rotations involved in the coordinate transformation, the number of the original voxels contributing to each of the transformed voxels will not be completely uniform, and therefore we expect that the noise will not be uniform across our subcubes. However, this should have a minimal effect in the propagated noise because subcube orientations are largely independent of each other.

In Fig. 3, we show a few examples of oriented individual subcubes where the neighbour (which is outside the image) is always located along the positive side of the x-axis at distances larger than 16 arcsec.

Finally, we stack all our subcubes applying an averaged-sigma-clipping algorithm with a single iteration discarding values above and below $\pm 3\sigma$, where σ is calculated for each voxel.

4 RESULTS

In the left-hand panel of Fig. 4, we present the pseudo-NB image of the oriented stack-cube using our full sample of subcubes. This image has been obtained by collapsing the stack-cube along five layers in the z-direction, i.e. 6.25 Å, centred on the peak of the galaxy Ly α emission.

The wavelength width of the pseudo-NB has been chosen to maximize the expected SNR taking into account the possible width of the intergalactic Ly α emission (e.g. Cantalupo et al. 2005) and wavelength shifts with respect to the LAE peak. We have experimented different NB wavelength widths and found that using five layers gives the best results both in terms of noise and detectability of Ly α emission as we will show in this section.

Clearly, there are no indications of significant emission at distances larger than 4 arcsec from the centre at the predicted position, i.e. the expected location of emitting filaments with respect to the central, LAE emission (indicated by the purple arrow). A closer look at the central part of the stack shows the presence of ring-like emission features and slight asymmetric emission distribution in the direction of the neighbouring galaxies (up to a scale of about 4 arcsec). The most prominent of the ring-like features is at a distance of 4 arcsec from the centre. In order to understand if these features are due to systematics in our stacking procedure we produced a set of 200 new stacks using the same sample of 390 subcubes obtained with *random* orientations. We combined these 200 randomly oriented stacks into a single 'super-random' stack in order to boost the systematic effects with respect to Poisson noise.

In the right-hand panel of Fig. 4, we show the resulting pseudo-NB image after subtracting this 'super-random' stack from the oriented one. We notice that the ring-like features present on the oriented stack are mostly suppressed suggesting a non-physical nature of this emission. Because a single LAE can be repeated in the stack several times at different orientations, any non-circularly symmetric emission can indeed appear as a ring-like feature in the final cube (notice that a single asymmetric object repeated at an infinite number of random orientations will create perfect rings). However, we

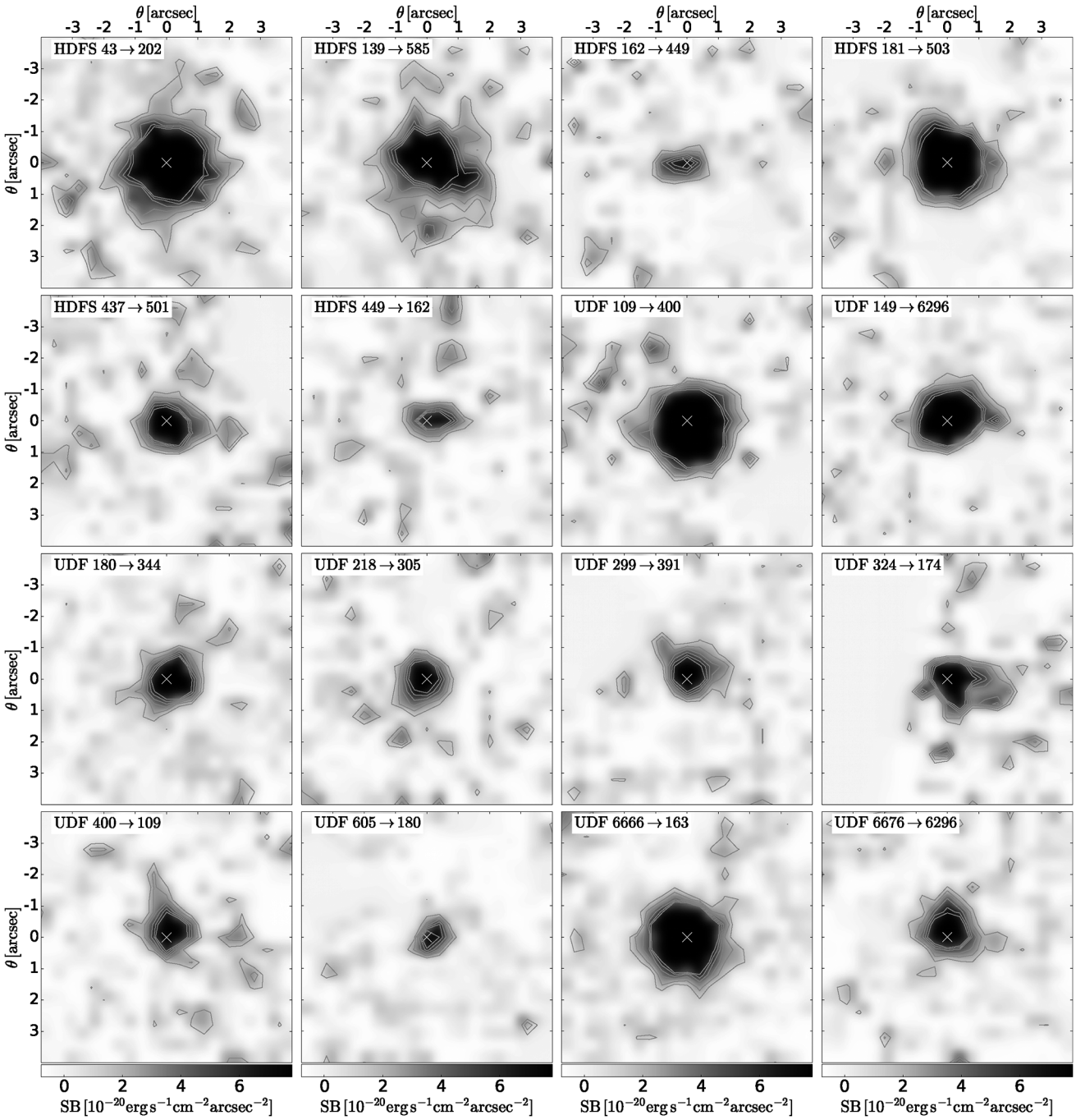

Figure 3. Examples of pseudo-NB images with a wavelength width of 6.25 Å obtained from the oriented and resampled subcubes. The label indicates the field and ids of the LAE, at the centre of the image, and its neighbour, located along the positive side of the *x*-axis (outside the image). The cross at the origin of coordinates represents the position of the peak of the Ly α emission. The images are smoothed with a Gaussian filter of $\sigma = 1$ pixel (0.4 arcsec) to improve visualization. Contour levels range from two to six times the noise levels of the smoothed image.

notice that the asymmetry in the emission towards the neighbouring galaxies in the light distribution remains.

In order to assess the significance of this asymmetry we examine the SB profile integrated over a spatial aperture of vertical height of 2 arcsec and increasing horizontal widths (from 0.4 to 2 arcsec) for both the oriented and 'super-random' stacks. In the left-hand panel of Fig. 5, we show as a black line the SB profile obtained for the oriented stack along the positive side of the *x*-axis (right direction) and as a blue line the same profile obtained for the 'super-random'. The shaded area represents the 2σ standard deviation of the average of the 'random' stacks. Notice that this value is well below the expected fluorescence from UVB (green line in Fig. 5) and therefore gives us constraints on either the value or the UVB or the presence of LLSs in our subcubes. The integrated 2σ limit considering a region of 1 arcsec^2 area between 6 and 12 arcsec corresponds to 0.44×10^{-20} erg s^{-1} cm^{-2} arcsec^{-2}, i.e. a factor of about 18 deeper than the individual cubes in the same spatial aperture and wavelength width (see e.g. Bacon et al. 2017). Notice

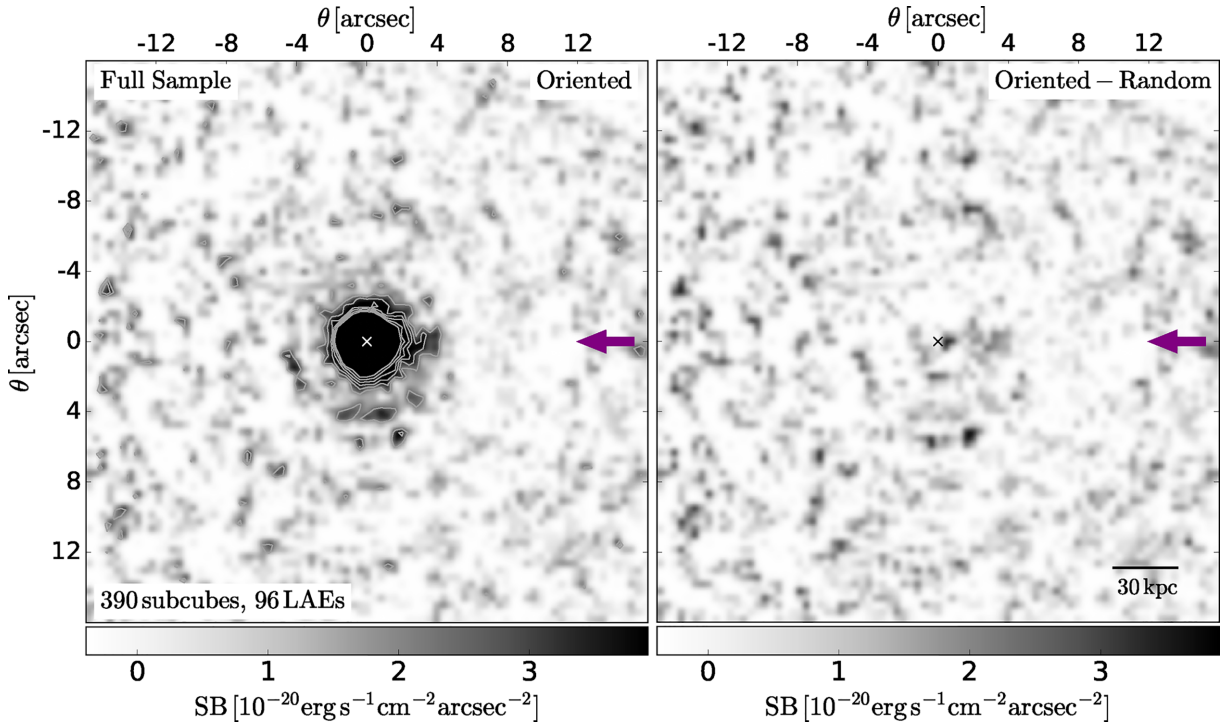

Figure 4. Left-hand panel: pseudo-NB image of the oriented stack using the full sample of subcubes. As in Fig. 3, the wavelength width of the images corresponds to 6.25 Å. The subcubes have been oriented in such a way that the galaxy neighbours are always positioned on the positive part of the x-axis at distances larger than 16 arcsec. The purple arrow indicates the expected position of filaments connecting neighbouring galaxies. Notice that the noise is not uniform and that it is higher on the negative part of the x-axis because of edge effects (since neighbours are always inside the cube, the edges will be on the negative x-axis side). Despite this effect, a clear asymmetry towards galaxy neighbours is present in the light distribution around the central galaxy. Right-hand panel: pseudo-NB image after subtracting a combination of randomly oriented stacks ('super-random' stack, see the text for details) from the oriented one presented in the left-hand panel. As expected, systematic effects (e.g. the ring-like structures present in the oriented stack) are significantly reduced in this image. However, the asymmetry in the central emission towards the neighbouring galaxies remains.

that this is consistent with the expected decrease for non-correlated noise given the amount of subcubes in our stack (i.e. a factor of 19.7). Under the extreme and unlikely hypothesis that all our galaxies are connected to each other by LLS filaments the limit given above is about a factor of 3 below the expected fluorescent Ly α SB from the HM12 UVB (1.14×10^{-20} erg s^{-1} cm^{-2} arcsec^{-2} at $z = 3.5$, see Section 1). We will discuss the implications of this result in Section 5.

Focusing again at the closest region around galaxies, we notice that the oriented stack shows excess emission between 3 and 4σ with respect to the 'random' orientation up to a scale of about 4 arcsec (corresponding to about 30 projected kpc at $z \sim 3.5$. The comparison of the SB profile in the opposite direction (right-hand panel of Fig. 5) shows no excess with respect to random orientations, reinforcing the hypothesis of a physical origin for the oriented CGM emission (see Section 5 for discussion).

Motivated by this result, we perform a new set of stacks splitting our sample into halves. The subcubes for each of the half-samples have been selected by looking at the median of the following observational properties of the LAEs (see Table 1): (i) line-of-sight comoving and projected (ii) distance to the neighbours, (iii) redshift, (iv) luminosity, and (v) number of neighbours per galaxy (within a distance range 0.5 cMpc $< d <$ 20 cMpc). In particular, we group together all the subcubes with values below and above the medians. In Fig. 6, we show the SB in the rectangular region indicated in the top panel (the region with the strongest asymmetric emission) for the full sample and for each of the subsamples. Among all the properties examined, splitting the sample by the number of neighbours shows the largest variation and, in particular, the subsample with a number of neighbours larger than 8 presents the brightest and most significant signal in the region of interest. In the top-left panel of Fig. 7, we present the pseudo-NB image obtained from this subsample compared to the other half of the sample (bottom-left panel) and the corresponding 'oriented-random' pseudo-NB image. The results obtained with the other subsamples are presented in the appendix A. It is worth noticing that, even though there are regions with an excess of emission which appear as significant as the one towards neighbours, they appear at random positions of our different stacks, whereas the oriented excess of emission in the region of interest is consistently present in all of our stacks (except for the stack with a number of neighbours lower than 8). This suggests that the most likely origin of these apparent sources is either noise or faint clumps randomly distributed. A particular case is at the centre of the subcubes, where the emission coming from the LAEs is maximal and, given that some LAEs are repeated several times in our subcubes, the number of independent pixels is small. In the central regions the expected variation between the oriented stacks and the random stacks will be driven mostly by the diversity of SB profiles among our sample of galaxies and any random asymmetries present on them.

In the left-hand panel of Fig. 8, we show the SB profile for the subsample of galaxies with number of neighbours larger than 8. As in Fig. 5, this profile has been obtained by integrating over a spatial aperture of vertical height of 2 arcsec and increasing horizontal widths (from 0.4 to 2 arcsec). Compared to the 'super-random' stack SB profile derived from the same subsample of galaxies, we

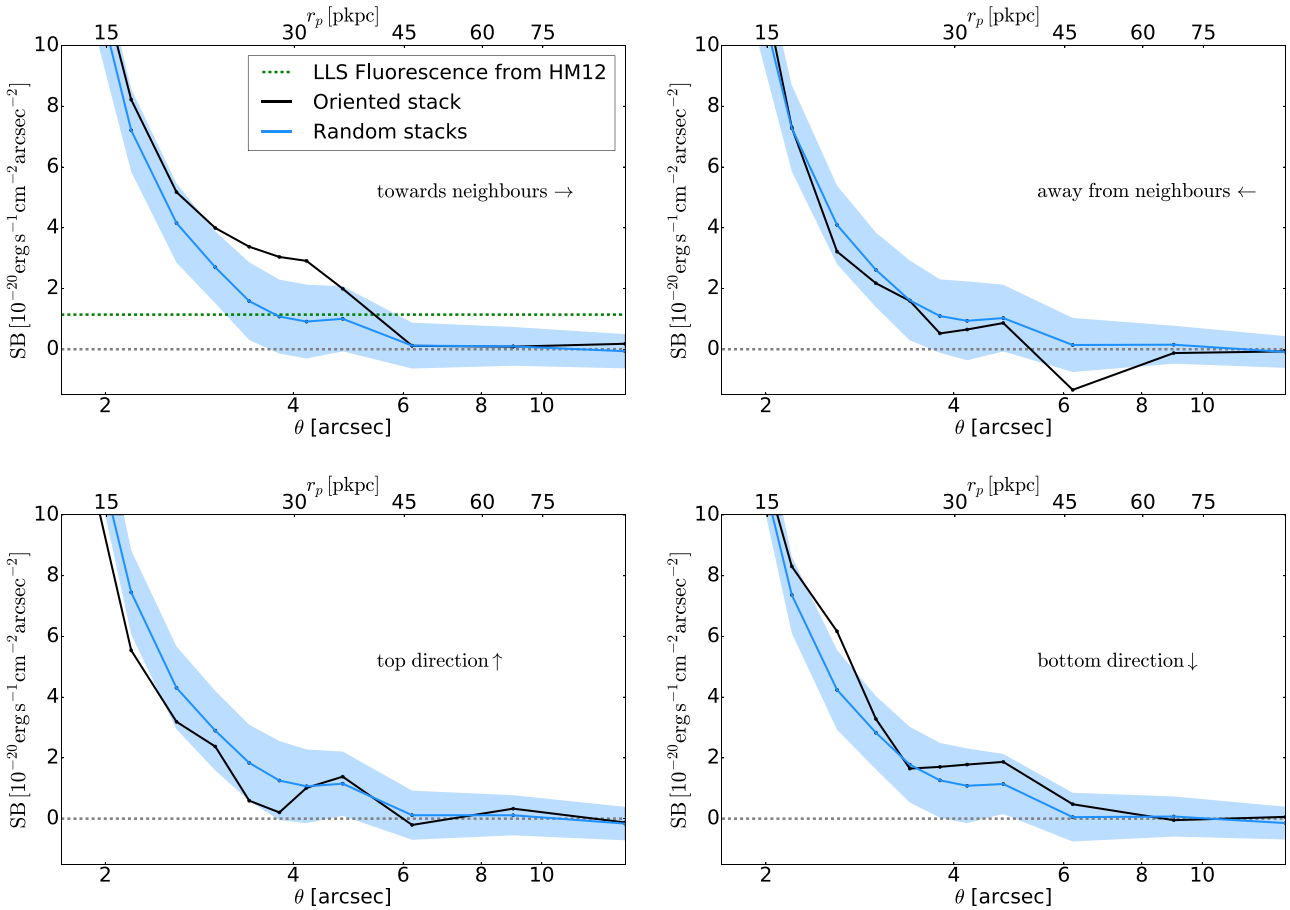

Figure 5. Top-left panel: SB profile of the oriented (black line) and 'super-random' (blue line) full-sample stacks obtained using apertures with increasing sizes (from 0.4 arcsec × 2 arcsec at the centre to 2 arcsec × 2 arcsec at θ larger than 10 arcsec). The oriented SB profile is calculated starting from the centre towards the neighbouring LAEs. The light blue shadowed areas represent the 2σ deviations from the average of the random stacks. The green dotted line indicates the expected Ly α fluorescent SB from LLSs illuminated by the Haardt & Madau (2012) UVB. A clear excess of emission in the oriented stack is present up to scales of about 4 arcsec (30 projected physical kpc) from the central galaxies compared to the randomly oriented stack. No significant emission is detected at scales larger than 5 arcsec up to 2σ levels that are well below the expected UVB fluorescence values. Top-right panel: SB profile in the direction opposite to the neighbours. There is no significant emission excess at any scales with respect to the randomly oriented stack. The excess is similarly not present when plotted against the vertical directions (bottom-left and right panels), and in general in any direction except the one towards neighbours. In relating θ to r_p, we assume all data points are at a median $z = 3.5$.

Table 1. Median values for the main properties of the full sample of subcubes included in our stack. Because some LAEs are repeated multiple times in our sample of subcubes, our median values are not the same as the ones from the selected sample of LAEs, but instead biased towards LAEs with more neighbours.

Property	Median value
Projected distance to the neighbour	32 arcsec
Comoving distance to the neighbour	8 Mpc
Redshift	3.5
Number of neighbours	8
Luminosity	9.1×10^{41} erg s^{-1}

clearly see an excess of emission between 2 and 4 arcsec at more than 3σ level at each spatial position. Note that a non-physical effect may give extra weight to some particular direction towards neighbour of certain LAEs. Indeed, given the small and rectangular field of view of MUSE, neighbours are more likely to be found along the diagonals of our data cube, especially if the LAEs are close to the FOV border. We will quantify the bias introduced by the FOV geometry and size by using larger MUSE data sets (e.g. the UDF-MOSAIC observations, see Bacon et al. 2017) in future work.

In order to assess if this 'oriented' excess of emission comes just from a small set of subcubes, we show in Fig. 9 the individual SB values in the region of interest for each of the oriented subcubes of both the full sample and the subsample with eight or more neighbours. The distribution of SB values is approximately Gaussian for both samples with very few outliers that do not contribute significantly to the overall emission. A closer look for the sample with eight or more neighbours shows a slight asymmetry on the positive part of the distribution at small SB values ($\sim 4 \times 10^{-20}$ erg s^{-1} cm^{-2} arcsec^{-2}) consistent with the measured emission in the stack.

5 DISCUSSION

The main results of our stacking analysis presented in the previous section are (i) a lack of detectable extended emission on IGM scales and (ii) the presence of a significant, statistical excess of CGM Ly α

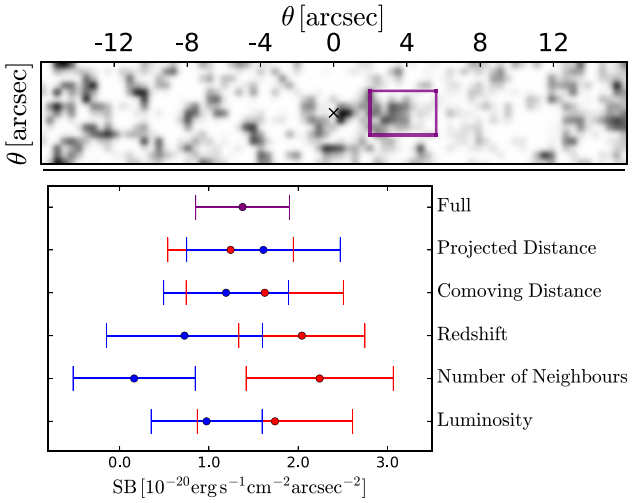

Figure 6. Top panel: image extracted from Fig. 4 indicating the region of excess emission (purple square) around galaxies in the oriented stack with respect to the 'super-random' one. Bottom panel: SB values within the region indicated above for each subsample of subcubes splitted by the median values of galaxies properties (see the text for details) and for the full sample. Among all the properties examined, splitting the sample by the number of neighbours shows the largest variation and, in particular, the subsample with a number of neighbours larger than 8 presents the brightest and most significant signal in the region of interest. The SB and the 1σ error bars are obtained by combining all randomly oriented stacks with a bootstrapping of the oriented stack (Fig. 4, left-hand panel), therefore it represents the excess of emission without the average CGM contribution. The red and blue dots represent subsamples with parameter values higher and lower than the median, respectively. The median values are: projected distance to the neighbour 32 arcsec, comoving distance to the neighbour 8 Mpc, redshift 3.5, number of neighbours 8 and luminosity 9.1×10^{41} erg s^{-1}.

emission in the direction of neighbouring galaxies up to distances of about 4 arcsec, i.e. about 30 projected kpc. In this section we discuss the implications of our results in the context of intergalactic structures around galaxies and the possible origin of the CGM emission excess.

5.1 LLSs and cosmic UVB constraints

As discussed in Section 1, our stacking analysis should maximize the detectability of intergalactic filaments illuminated by the cosmic UVB in the hypothesis that a significant fraction of the galaxies in our sample are connected to each other by filaments with column densities similar or higher than LLSs. Note that because of the particular geometry of the observed volume in our survey (limited to $\sim 450 \times 450$ kpc^2 in the plane of the sky) the majority of our galaxies may be connected to other sources that are *outside* our field of view. Therefore, those galaxies and corresponding subcube orientations may be missing in our stacking analysis.

Indicating with $f_{\rm conn}$ the fraction of possible galaxy-neighbour orientations with LLS filaments, our result should provide an upper limit on the product of $f_{\rm conn}$ and the cosmic UVB photoionization rate ($\Gamma_{\rm H\,I}$). In the extreme and unlikely case that $f_{\rm conn} = 1$, then we would obtain a 2σ upper limit of $\Gamma_{\rm H\,I} = 0.2 \times 10^{-12}$ s^{-1}. This value is about a factor of 3 below the HM12 and four times below the latest empirical estimates based on the comparison of the Ly α forest mean flux with cosmological simulations (e.g. Becker & Bolton 2013)[2] .

How can we constrain the possible value of $f_{\rm conn}$ and the spatial distribution of LLS around our galaxies? From an observational perspective, we can compare the estimates of the incidence of LLSs per line of sight and redshift $dn/dz \sim 1.5$ at $z \sim 3.5$ (Prochaska et al. 2010) with the number of galaxy-neighbour orientations in our sample.

Let us first hypothesize that each one of our galaxies is surrounded by a circularly symmetric distribution of gas with the column density of LLSs and that no other regions in our data cubes are covered by LLSs, i.e. that $f_{\rm conn} = 0$. In order to reproduce the observed dn/dz we would therefore require that each of the 96 galaxies in our sample, plus the 11 galaxies with a high-confidence flag that were discarded by our neighbouring-distance selection criteria, should be surrounded by a LLS with a radius of about 6 arcsec. If this were the case, then we should have been able to detect fluorescent emission from the UVB up to this radius at every possible angle around our galaxies. Figs 5 and 8 do not show evidence for an excess extending up to 6 arcsec with values compatible with the UVB and therefore LLSs cannot all be confined into circular regions around our galaxies. We notice, however, that there is an excess up to about 5 arcsec in the stack made with randomly oriented subcubes. In the conservative hypothesis that this is due to fluorescence from the HM12 UVB instead of being produced by processes related to the central galaxies, we would obtain a dn/dz that is slightly larger than half of the observed value. Therefore, unless un-detected faint galaxies substantially contribute to dn/dz, we think that it is likely that $f_{\rm conn}$ is not equal to zero.

On the other end, if we assume that the HM12 UVB is correct, we can use our result to provide a 2σ upper limit on $f_{\rm conn} \approx 0.3$. We notice that restricting the sample to the half of the subcubes at smaller neighbouring distances (up to 8 cMpc) or splitting the sample in two halves based on other galaxy properties (see Appendix A) does not give any detectable intergalactic emission and therefore we cannot obtain a better constraint on $f_{\rm conn}$. However, the increased noise of these subsamples do not allow a detailed analysis as in the case of the full sample. We will repeat this split-sample analysis in the future with the new, much larger sample of LAE emitters that will be detected in the UDF mosaic region (see e.g. Bacon et al. 2017; Leclercq et al. 2017) and we will include an analysis of cosmological simulations to guide our stacking analysis and to better constrain the value of $f_{\rm conn}$.

5.2 Origin of the oriented CGM emission excess

The analysis of the SB profile of the oriented stack for the full sample revealed a significant excess of emission towards galaxy neighbours with respect to the 'random' stacks (see Fig. 5) up to distances of about 4 arcsec from the galaxies. This excess is more pronounced when the stack is performed on the subsample of subcubes that are surrounded by the largest number of neighbours (see Fig. 8). What is the origin of this 'statistical excess' of oriented CGM emission?

[2] Possibly by coincidence our 2σ upper limit for $f_{\rm conn} = 1$ is close to the HM12 estimates based on a model that includes only quasars. Taken a face value, this would imply a Lyman-continuum escape fraction from galaxies at $z \sim 3.5$ close to zero and therefore such a model would have serious problems for Hydrogen reionization if this result would be extended to higher redshifts.

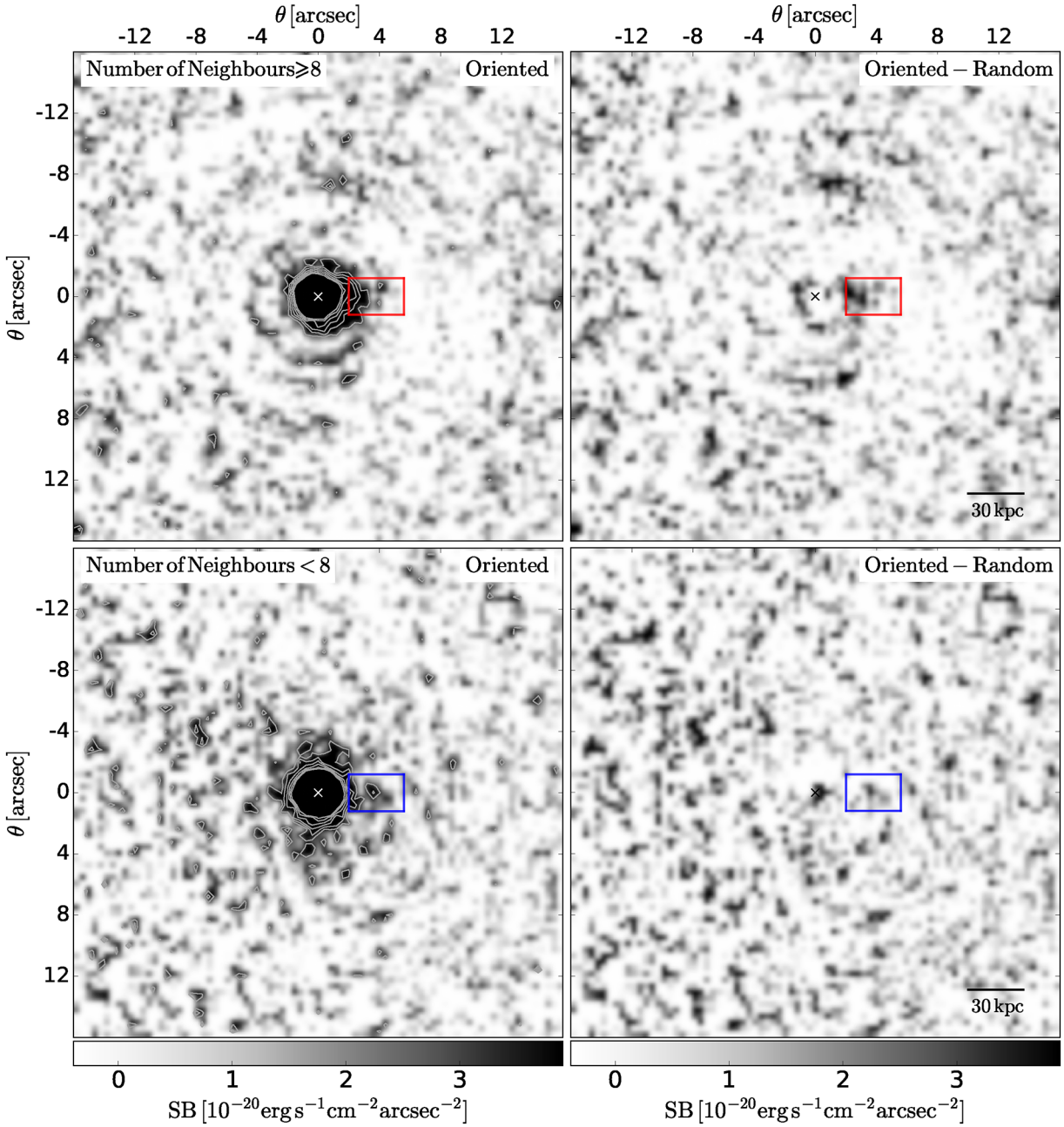

Figure 7. As in Fig. 4 but for the subsamples of subcubes with number of neighbours larger (top panels) and smaller (bottom panels) than the median value (8). The red and blue squares indicate the region of excess emission examined in Fig. 6.

We first consider the possibility that this excess is due to the Ly α emission from aligned and undetected satellite galaxies with Ly α fluxes below the detection limit. Using the results of Wisotzki et al. (2016) and Leclercq et al. (2017), we know that the circularly averaged UV emission from galaxies can be described by an exponential profile with a typical scale length of $r_{\rm UV} \sim 0.3$ kpc. If this extended UV profile contains the contribution of undetected satellites then we expect that their Ly α emission should be at least a few orders of magnitude below the observed value in our stack at a distance of 4 arcsec, i.e. 30 projected kpc, from the central galaxy in the direction of the neighbours. This applies also in the extreme case in which we place all the possibly undetected satellite galaxies in the region of excess emission (see Fig. 6). In this calculation, we have assumed that the equivalent width (EW) of the undetectable satellite galaxies is similar to the measured EW of our galaxies (assuming EW $\equiv$ SB$_{\rm Ly\,\alpha}$/SB$_{\rm UV}$, see a more detailed calculation in Appendix B). In order to obtain the observed Ly α emission in the region of excess emission, the EW of the satellite galaxies should have been much larger than what normal stellar population could produce (see Cantalupo et al. 2012 for discussion) and therefore we exclude a satellite-galaxy origin for this excess emission (see e.g. Lake et al. 2015; Mas-Ribas et al. 2017, for a more detail analysis on the contribution of unresolved satellite sources).

As an alternative possibility, let us consider the hypothesis that the CGM Ly α emission is produced by fluorescence due to the photons from the central galaxies. Given the average Ly α luminosities of

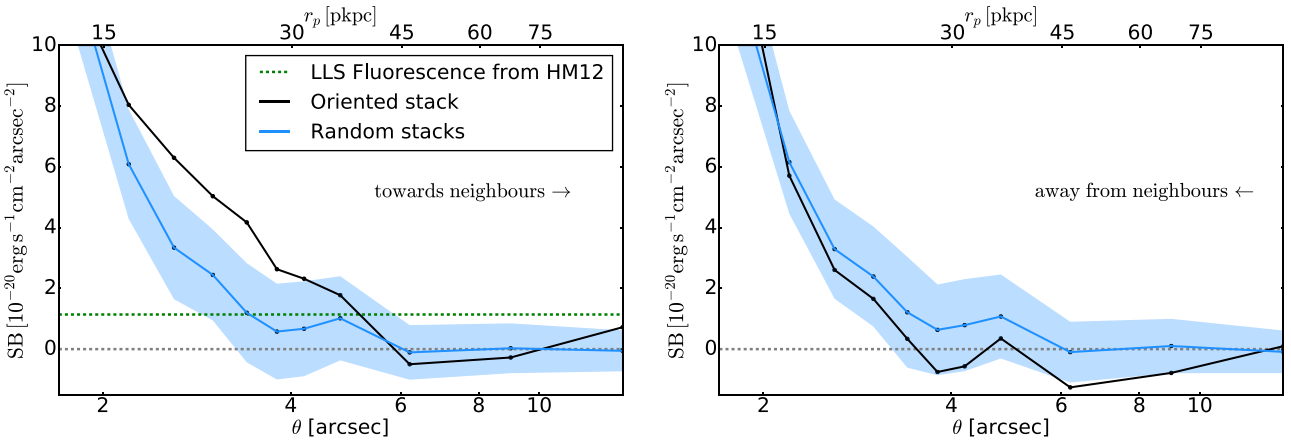

Figure 8. Same as Fig. 5 but for the subsample of subcubes with eight or more neighbours. As with the full sample, we clearly see an excess of emission in the oriented stack compared to random orientations, but now extended between 2" and 4" at more than 3σ level at each spatial position.

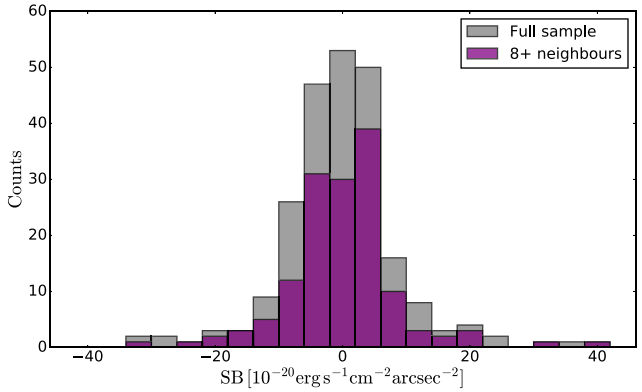

Figure 9. Distribution of SB in the aperture defined in Fig. 6 for each individual subcube in the full sample (grey) and the sample with eight or more neighbours (purple).

our sample ($\sim 10^{42}$ erg s^{-1}) we expect average star formation rates of about 0.6 $M_\odot$ yr^{-1} (using the standard SFR to Hα conversion factors and assuming Case B recombination line ratios between Hα and Lyα) and therefore intrinsic ionization rates of about $10^{53.5}$ photon s^{-1} (from STARBURST99 assuming continuous SFR and an age larger than 10^7 yr, Leitherer et al. 1999). To explain the observed Lyα SB at 30 projected kpc in the oriented stack ($\approx 3 \times 10^{-20}$ erg s^{-1} cm^{-2} arcsec^{-2}) with galaxy-fluorescence emission for self-shielded gas, we estimate that a Lyman-continuum escape fraction from the galaxy's Interstellar Medium of $f_{\rm esc}^{\rm ISM} \sim 2 \times 10^{-2}$ would be sufficient (for more details on the calculations see Appendix C). We notice that this escape fraction is an upper limit of the measurable escape fraction because it does not include absorption by the CGM. Although there are no direct measurements of Lyman-continuum photons escaping from high-z galaxies, a value of $f_{\rm esc}^{\rm ISM} \sim 2 \times 10^{-2}$ is totally consistent with current upper limits (see e.g. Iwata et al. 2009; Ono et al. 2010; Siana et al. 2015) and with the required value for the reionization of hydrogen (see e.g. HM12). Larger values of $f_{\rm esc}^{\rm ISM}$ can produce highly ionized gas. In this case, the expected fluorescent SB will scale with the gas density squared. The excess of emission towards the galaxy neighbours could then be simply explained by an increased gas density along this direction. In particular, the increased SB in the oriented stack by a factor of about 3 with respect to the 'random' stack would imply statistically higher densities by a factor of about 1.7 towards the galaxy neighbours.

If the Lyα emission is due to scattering in a neutral medium instead of fluorescence, our result would again imply that CGM densities towards galaxy neighbours should be statistically larger than in any other direction. We note, however, that the lack of a correlation between Lyα/UV luminosities and halo exponential scale lengths does not clearly favour a scattering scenario (see e.g. Wisotzki et al. 2016; Leclercq et al. 2017).

In both cases, an increased density on scales of 30 projected kpc around galaxies in the direction of much more distant neighbours (on average, 10 comoving Mpc) seems a surprising result for which a detailed comparison with simulations will be needed. As discussed in Section 4, we do not detect any correlation between the strength of this oriented CGM excess emission and any properties of the galaxies, including neighbour-distances, with the exception of the environment, as measured using the number of neighbours. A possible origin of this trend may be due to the larger dark matter haloes of the more clustered LAEs that therefore could have larger and denser filaments in their circumgalactic environments. If the CGM excess is connected to the distribution of gas on IGM scales, e.g. cosmological filaments, then the derived densities above will be degenerate with the value of $f_{\rm conn}$. In particular, we expect that the implied densities due to fluorescence or Lyα scattering in the direction of the neighbours will scale as $f_{\rm conn}^{-1}$. Another dilution effect of the expected signal in our stacking analysis, on both CGM and IGM scales, could be due to the possibility that filaments are bended. Also in this case, a detailed comparison with simulations will be needed to assess the importance of these effects for the implications of our results.

6 SUMMARY

Cosmological simulations suggest that the gas distribution between galaxies is filamentary and that the filaments are oriented preferentially towards neighbouring galaxies (e.g. Gheller et al. 2015), a property that can be intimately linked to the initial conditions of the cosmic density field (e.g. Bond et al. 1996). Illuminated by the cosmic UVB, these filaments are expected to emit fluorescent Lyα radiation with SB levels that are, unfortunately, one or two orders of magnitude below current observational limits for individual detections.

We presented and developed the idea of an 'oriented stacking' approach using Ly α LAEs away from quasars at redshift $3 < z < 4$ detected in deep MUSE cubes. We stacked three-dimensional regions (subcubes) around LAEs in the HDFS and UDF-10 MUSE fields (Bacon et al. 2015, 2017) with orientations determined by the position of LAE neighbours within a line-of-sight comoving distance of $0.5 < d < 20$ cMpc (assuming pure Hubble flow). If neighbouring galaxies are connected by filaments and these filaments are LLSs, then our oriented-stacking method should boost the SNR of UVB-induced Ly α fluorescence by about the square root of the number of stacking elements.

By stacking 390 individual, 're-oriented' subcubes we achieved a 3σ sensitivity level of SB $\approx 0.78 \times 10^{-20}$ erg s^{-1} cm^{-2} arcsec^{-2} in an aperture of 0.4 arcsec^2 for a pseudo-NB of width 6.25 Å, three times below the expected fluorescent signal from the values of the cosmic UVB at $z \sim 3.5$ estimated by HM12 in the extreme hypothesis that all our galaxies are connected to each other by LLS filaments. No detectable emission is found on intergalactic scales (i.e. at distances larger than 40 and up 120 projected kpc from galaxies) at significant levels, implying that at least two thirds of our subcubes should not contain oriented LLSs for a HM12 cosmic UVB. This result is independent of all galaxy properties that we have investigated in this study (projected and comoving distances from neighbours, redshifts, numbers of neighbours and luminosities).

However, significant emission is detected in the CGM of galaxies (up to about 30 projected kpc) at SB levels of $\approx 3 \times 10^{-20}$ erg s^{-1} cm^{-2} arcsec^{-2} in the direction of galaxy neighbours but not in other directions.

The signal is stronger (4σ level) at radii up to 4 arcsec when the sample is splitted considering only the galaxies with a number of neighbours equal or larger than 8, while it seems independent of any of the other galaxy properties mentioned above. We investigated the possible origin of this excess emission and we found that 'preferentially oriented' Ly α emission from un-detected satellite galaxies is at least two orders of magnitude below the observed value. We estimated that a very modest escape fraction of Lyman-continuum photons from the ISM of the central galaxies (i.e. $f_{\rm esc}^{\rm ISM} \sim 2 \times 10^{-2}$) should be sufficient to produce enough Ly α emission by photoionizing at least part of the CGM up to 30 kpc. In this case, the excess of CGM emission towards the galaxy neighbours can simply be explained by an increased gas density along this direction by a factor of about 2, on average. The dependence of this excess on the galaxy environments may suggest a connection with the host halo of the LAEs in terms of filament sizes and densities.

The methods and the idea developed in this first study will be extended in several directions in future works with the goal of understanding the origin and nature of the oriented CGM emission excess and to provide better constraints on the presence and properties of intergalactic filaments. In particular, we plan to increase the observational sample of LAEs for our stacking analysis with the new catalogues and data in the MUSE UDF-mosaic region (Bacon et al. 2017) and other MUSE cubes with similar exposure times. This new data will provide a one order of magnitude increase in the number of galaxies and spatial coverage, albeit at a lower sensitivity level (10 h exposure time per field, versus the 30 h per field used in this study). At the same time, we plan to use high-resolution cosmological simulations to guide future stacking analyses by estimating the probability that galaxies with given properties are connected by LLSs. A positive detection would provide constraints on the morphological and physical properties of the Cosmic Web away from quasars and, at the same time, a direct measurement of the amplitude of the cosmic UVB at high redshift.

ACKNOWLEDGEMENTS

This work has been supported by the Swiss National Science Foundation. In particular, SC gratefully acknowledges support from Swiss National Science Foundation grant PP00P2_163824. LW acknowledges funding by the Competitive Fund of the Leibniz Association through grant SAW-2015-AIP-2. ERC Grant agreement 278594-GasAroundGalaxies.

REFERENCES

Arrigoni Battaia F., Hennawi J. F., Cantalupo S., Prochaska J. X., 2016, ApJ, 829, 3
Bacon R. et al., 2010, Proc. SPIE, 7735, 773508
Bacon R. et al., 2015, A&A, 575, A75
Bacon R. et al., 2017, A&A, 608, A1
Bajtlik S., Duncan R. C., Ostriker J. P., 1988, ApJ, 327, 570
Becker G. D., Bolton J. S., 2013, MNRAS, 436, 1023
Bennett C. L., Larson D., Weiland J. L., Hinshaw G., 2014, ApJ, 794, 135
Bolton J. S., Haehnelt M. G., Viel M., Springel V., 2005, MNRAS, 357, 1178
Bond J. R., Kofman L., Pogosyan D., 1996, Nature, 380, 603
Borisova E. et al., 2016, ApJ, 831, 39
Calverley A. P., Becker G. D., Haehnelt M. G., Bolton J. S., 2011, MNRAS, 412, 2543
Cantalupo S., 2017, in Fox A., Davé R., eds, Astrophysics and Space Science Library, Vol. 430, Gas Accretion onto Galaxies. Springer-Verlag, Berlin, p. 195
Cantalupo S., Porciani C., Lilly S. J., Miniati F., 2005, ApJ, 628, 61
Cantalupo S., Porciani C., Lilly S. J., 2008, ApJ, 672, 48
Cantalupo S., Lilly S. J., Haehnelt M. G., 2012, MNRAS, 425, 1992
Cantalupo S., Arrigoni-Battaia F., Prochaska J. X., Hennawi J. F., Madau P., 2014, Nature, 506, 63
Carswell R. F., Webb J. K., Baldwin J. A., Atwood B., 1987, ApJ, 319, 709
Conseil S., Bacon R., Piqueras L., Shepherd M., 2016, preprint (arXiv:1612.05308)
Dall'Aglio A., Wisotzki L., Worseck G., 2008, A&A, 480, 359
Faucher-Giguère C.-A., Lidz A., Hernquist L., Zaldarriaga M., 2008, ApJ, 688, 85
Faucher-Giguère C.-A., Lidz A., Zaldarriaga M., Hernquist L., 2009, ApJ, 703, 1416
Gheller C., Vazza F., Favre J., Brüggen M., 2015, MNRAS, 453, 1164
Gould A., Weinberg D. H., 1996, ApJ, 468, 462
Haardt F., Madau P., 1996, ApJ, 461, 20
Haardt F., Madau P., 2012, ApJ, 746, 125 (HM12)
Haiman Z., Rees M. J., 2001, ApJ, 556, 87
Hennawi J. F., Prochaska J. X., Cantalupo S., Arrigoni-Battaia F., 2015, Science, 348, 779
Hogan C. J., Weymann R. J., 1987, MNRAS, 225, 1P
Inami H. et al., 2017, A&A, 608, A2
Iwata I. et al., 2009, ApJ, 692, 1287
Kennicutt R. C., Jr, et al., 2009, ApJ, 703, 1672
Kollmeier J. A., Zheng Z., Davé R., Gould A., Katz N., Miralda-Escudé J., Weinberg D. H., 2010, ApJ, 708, 1048
Lake E., Zheng Z., Cen R., Sadoun R., Momose R., Ouchi M., 2015, ApJ, 806, 46
Leclercq F. et al., 2017, A&A, 608, A8
Leitherer C. et al., 1999, ApJS, 123, 3
Libeskind N. I., Tempel E., Hoffman Y., Tully R. B., Courtois H., 2015, MNRAS, 453, L108
Mas-Ribas L., Dijkstra M., Hennawi J. F., Trenti M., Momose R., Ouchi M., 2017, ApJ, 841, 19
Noterdaeme P., Petitjean P., Pâris I., Cai Z., Finley H., Ge J., Pieri M. M., York D. G., 2014, A&A, 566, A24
Ono Y., Ouchi M., Shimasaku K., Dunlop J., Farrah D., McLure R., Okamura S., 2010, ApJ, 724, 1524
Peebles P. J. E., Groth E. J., 1975, ApJ, 196, 1

Peroux C., McMahon R. G., Storrie-Lombardi L. J., Irwin M. J., 2003, MNRAS, 346, 1103
Prochaska J. X., O'Meara J. M., Worseck G., 2010, ApJ, 718, 392
Rauch M., 1998, ARA&A, 36, 267
Rauch M. et al., 1997, ApJ, 489, 7
Rauch M. et al., 2008, ApJ, 681, 856
Scott J., Bechtold J., Dobrzycki A., Kulkarni V. P., 2000, ApJS, 130, 67
Siana B. et al., 2015, ApJ, 804, 17
Steidel C. C., Bogosavljević M., Shapley A. E., Kollmeier J. A., Reddy N. A., Erb D. K., Pettini M., 2011, ApJ, 736, 160
van de Voort F., Schaye J., 2013, MNRAS, 430, 2688
Wisotzki L. et al., 2016, A&A, 587, A98
Xue R. et al., 2017, ApJ, 837, 172

APPENDIX A: HALF STACKS

In this section, we present the pseudo-NB images for the subsample of subcubes splitted by the following galaxy properties (see Table 1): (i) luminosity (Fig. A1), (ii) redsfhit (Fig. A2), (iii) comoving line-of-sight distance (Fig. A3), and (iv) projected distance (Fig. A4).

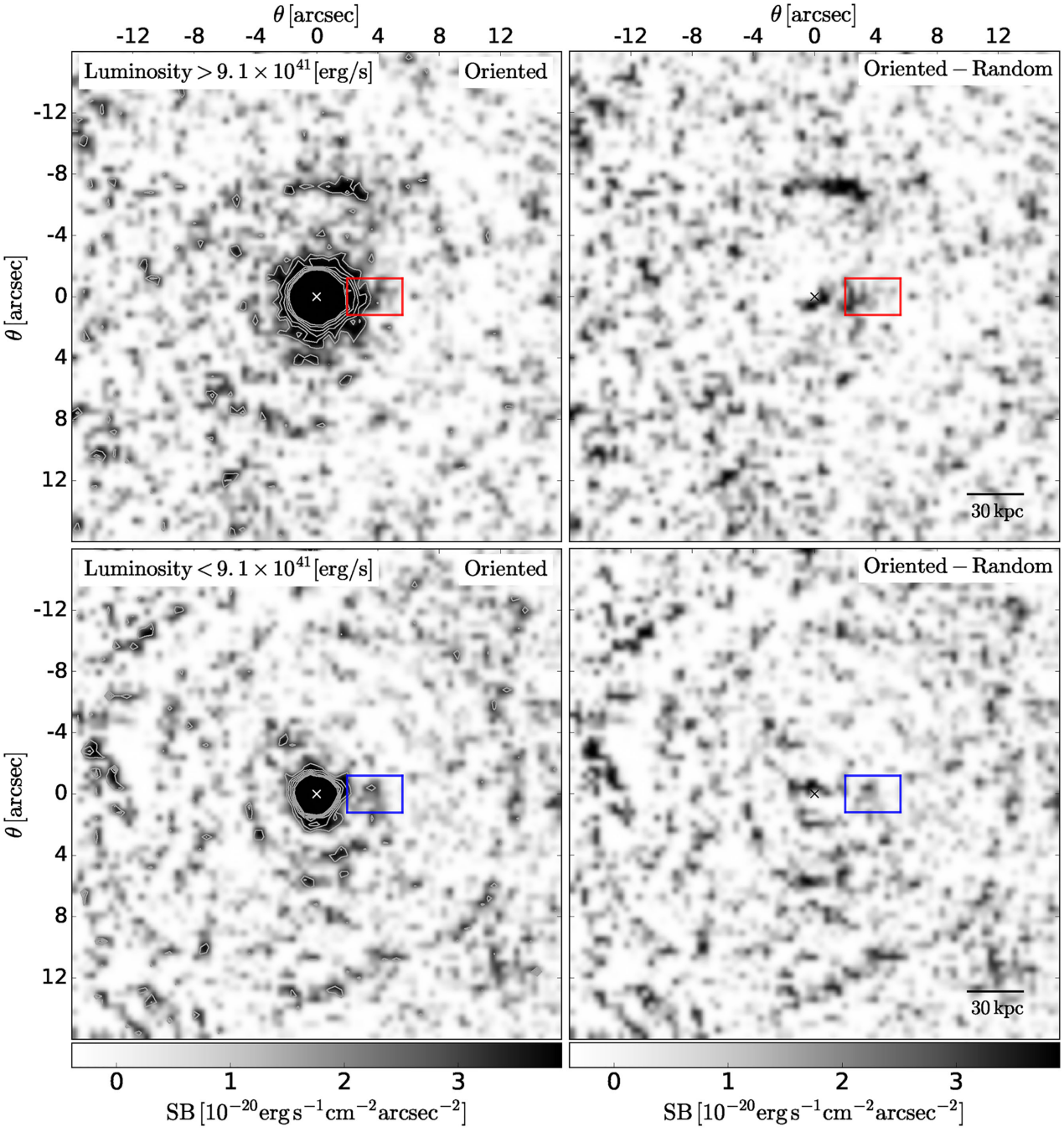

Figure A1. Same as Fig. 7 for a median luminosity of 9.1×10^{41} erg s^{-1}.

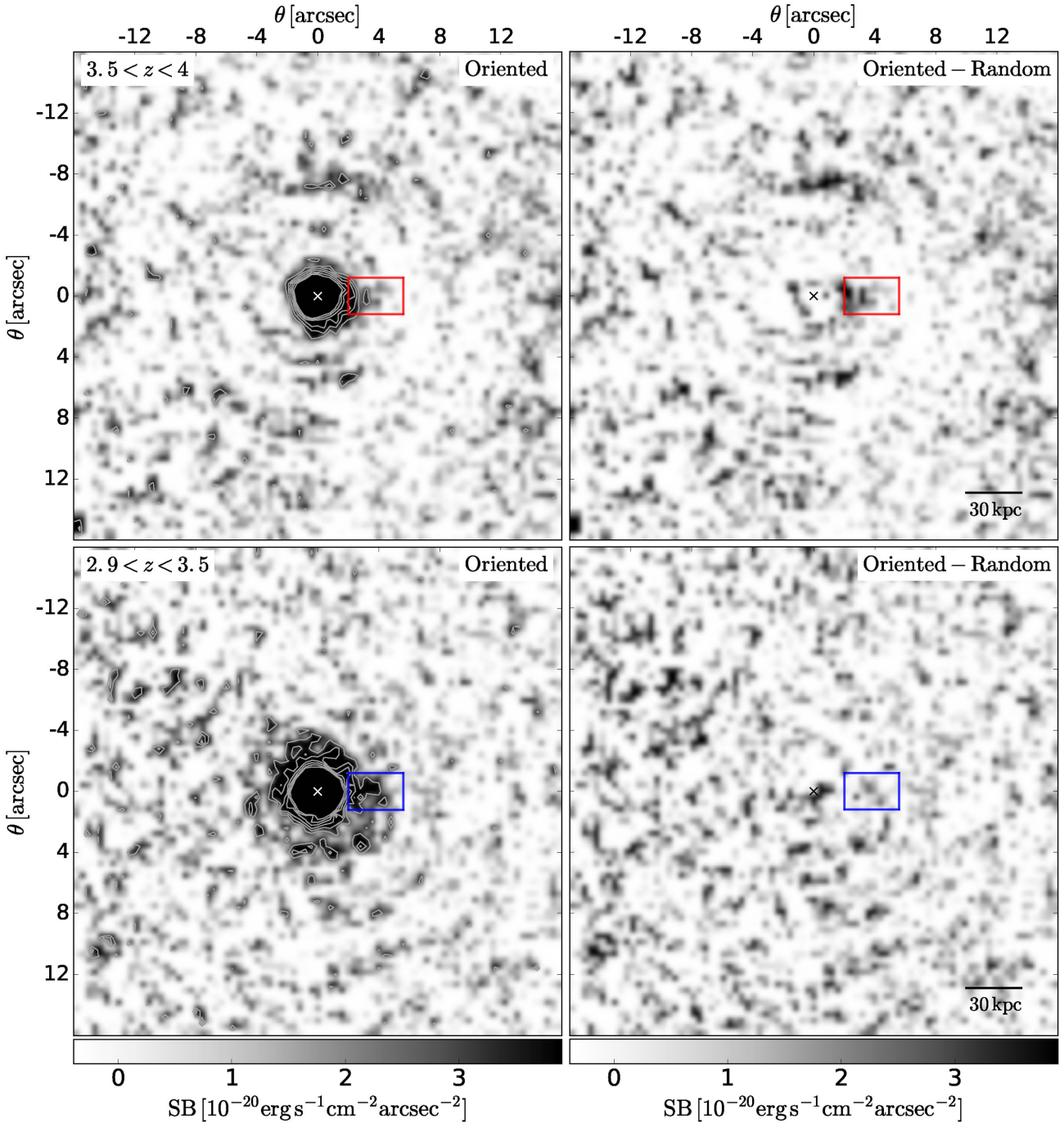

Figure A2. Same as Fig. 7 for a median redshift of $z = 3.5$.

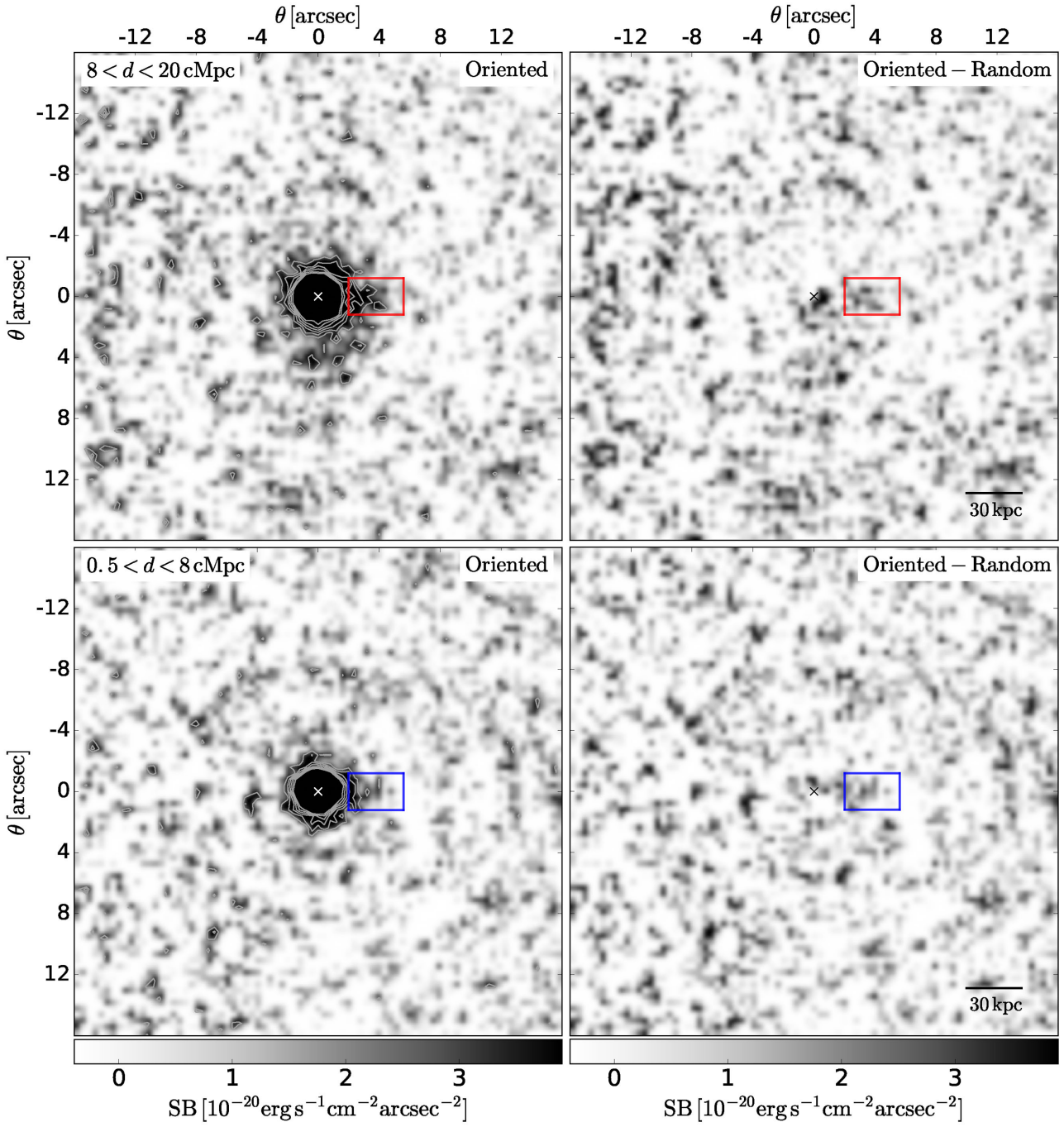

Figure A3. Same as Fig. 7 for a median comoving distance to the neighbour of 8 cMpc.

APPENDIX B: CONTRIBUTION FROM SATELLITE GALAXIES ON THE CGM EXCESS EMISSION

As described in Section 5.2, the analysis of the SB profile of the oriented stack for the full sample shows a significant excess of emission towards galaxy neighbours with respect to the 'random' stacks, up to distances of about 4 arcsec from galaxies. Here, we present in detail the calculations made to exclude that this excess is due to the Ly α emission from aligned satellite galaxies with Ly α fluxes below the detection limit.

We test the 'satellite-galaxy' hypothesis for the excess emission by assuming the extreme case in which satellite galaxies present around LAEs are concentrated in the region of our 'oriented stack' in the direction of galaxy neighbours, i.e. within a 'vertical height' of 2 arcsec. This means that any continuum emission present in studies that looked at averaged circularly symmetric profiles will be boosted in our case by a factor $f = 4\pi$ at $r = 4$ arcsec. Using the results of Wisotzki et al. (2016) and Leclercq et al. (2017), we know that the circularly averaged UV emission from galaxies can be described by an exponential profile with a typical scale length of $r_{\rm UV} \sim 0.3$ kpc. We assume that the extended UV emission in this

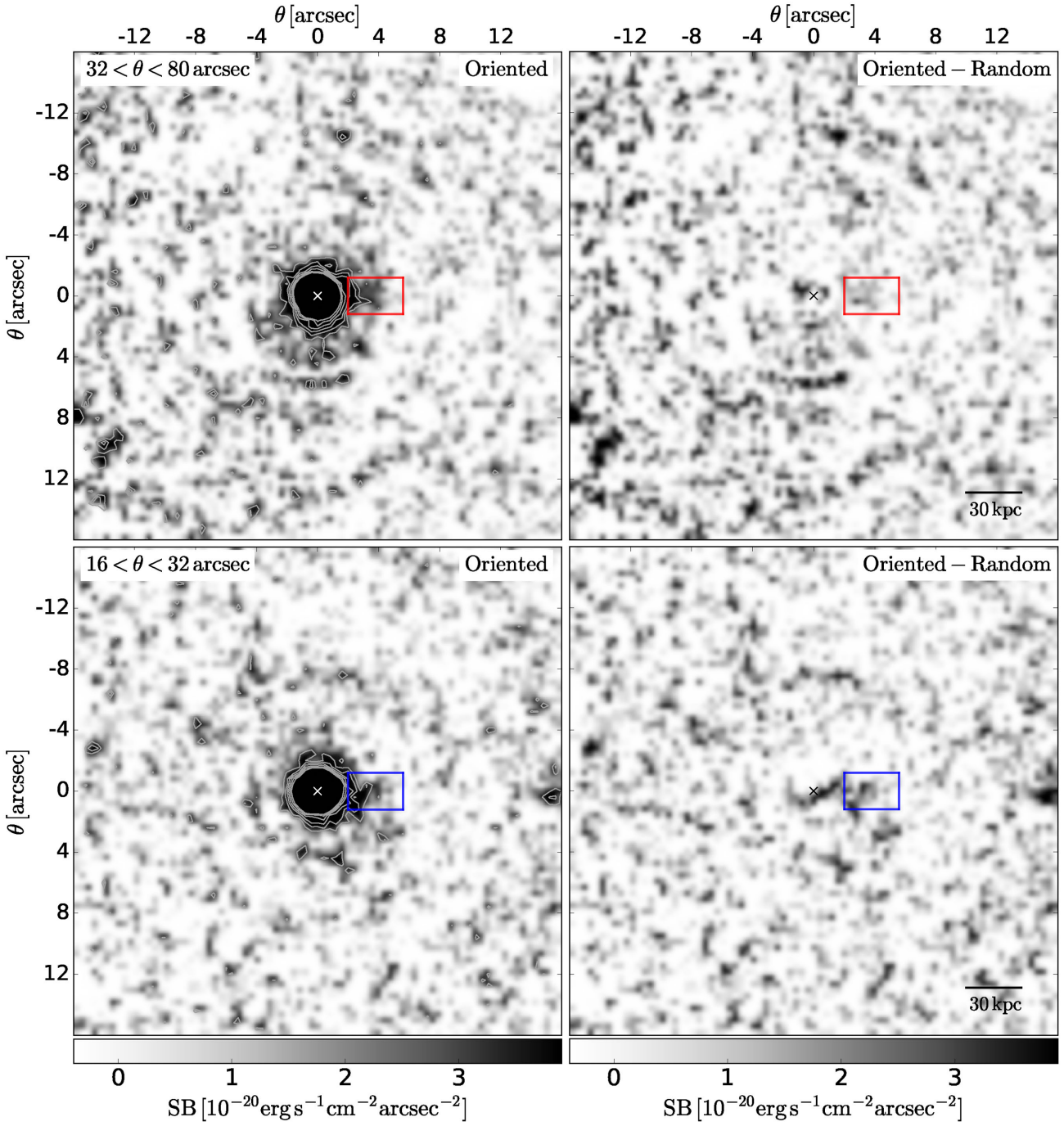

Figure A4. Same as Fig. 7 for a median projected distance to the neighbour of 32 arcsec.

profile is due to undetected UV satellites. How much Ly α emission can these satellites produce at 4 arcsec, i.e. 30 projected kpc? Using the definition of equivalent width, EW $\equiv$ SB$_{\mathrm{Ly}\,\alpha}$/SB$_{\mathrm{UV}}$ (where SB$_{\mathrm{UV}}$ is the SB per Å of the UV continuum), we obtain:

$$\mathrm{SB}^{\mathrm{sat}}_{\mathrm{Ly}\alpha}(r) = f \times \mathrm{EW} \times \mathrm{SB}_{\mathrm{UV},0}\,\exp(-r/r_{\mathrm{UV}}), \quad \text{(B1)}$$

where f is the geometrical factor defined above and SB$_{\mathrm{UV},0}$ is the peak of UV emission at the centre of the galaxy. Using again the definition of EW we can re-write equation (B1), as

$$\mathrm{SB}^{\mathrm{sat}}_{\mathrm{Ly}\alpha}(r) = f \times \mathrm{SB}_{\mathrm{Ly}\alpha,0}\,\exp(-r/r_{\mathrm{UV}}), \quad \text{(B2)}$$

where we have assumed that the EW of the central and satellite galaxies are the same and SB$_{\mathrm{Ly}\,\alpha,0}$ is now the observed central SB of our stack. Because this is a difficult quantity to measure precisely in our stack, we substitute SB$_{\mathrm{Ly}\,\alpha,0}$ in the previous equation with the observed SB at a radius of 2 arcsec (i.e. 10^{-19} erg s^{-1} cm^{-2} arcsec^{-2}) using the same formalism above. Using these values, we obtain the expected Ly α SB from satellite galaxies at 4 arcsec:

$$\mathrm{SB}^{\mathrm{sat}}_{\mathrm{Ly}\alpha}(r = 4\,\mathrm{arcsec}) = 1.27 \times 10^{-22}\mathrm{erg\,s^{-1}cm^{-2}arcsec^{-2}}\,. \quad \text{(B3)}$$

Because SB$^{\mathrm{sat}}_{\mathrm{Ly}\alpha}(r = 4$ arcsec) is more than two orders of magnitude below the observed Ly α SB in the oriented stack ($\sim 3 \times 10^{-20}$ erg

s^{-1} cm^{-2} $arcsec^{-2}$), we can exclude a satellite-galaxy origin for this excess emission with respect to the 'random' stack.

APPENDIX C: LYMAN-CONTINUUM ESCAPE FRACTION FROM GALAXIES

As a first order calculation of the escape fraction of Lyman-continuum photons from the ISM of galaxies, we compare the expected Ly α photons produced by photons coming from the central galaxy ($\Gamma_{\rm gal}$) with the observed Ly α SB at 30 kpc from the galaxy ($\Gamma_{\rm obs}$), where the excess of emission was found. The escape fraction will be given by

$$f_{\rm esc}^{\rm ISM} = \Gamma_{\rm obs}/\Gamma_{\rm gal}. \quad \text{(C1)}$$

We can obtain $\Gamma_{\rm gal}$ by converting the typical Ly α luminosity in our LAE sample (10^{42} erg s^{-1}) into a SFR and therefore to $\Gamma_{\rm gal}$ in the fluorescent recombination case. Using a standard Ly α to H α ratio for case B recombination of Ly α/H α = 8.7, and the following L(H α) to SFR conversion relation

$$\mathrm{SFR}(\mathrm{H}\,\alpha) = 5.5 \times 10^{-42} L(\mathrm{H}\,\alpha) \quad \text{(C2)}$$

(e.g. Kennicutt et al. 2009), we obtain a SFR of 0.6 $M_\odot$ yr^{-1}. Assuming a continuous SFR and a stellar-population age older than 10^7 yr from STARBURST99 (Leitherer et al. 1999) we obtain an intrinsic ionization rate $\Gamma_{\rm ion} \sim 10^{53.5}$ photon s^{-1}. About 60 per cent of the photons should be converted to Ly α for case B recombination (e.g. Cantalupo, Porciani & Lilly 2008) and therefore $\Gamma_{\rm gal} = 0.6\,\Gamma_{\rm ion}$.

$\Gamma_{\rm obs}$ is obtained from the observed SB, applying a SB dimming correction of $(1+z)^4$ integrated over the full surface of the sphere and divided by the energy of the Ly α photon,

$$\Gamma_{\rm obs}(r,z) = 4\pi\, r^2\, (1+z)^4\, \mathrm{SB}(r)/h\, \nu_{\rm Ly\alpha}. \quad \text{(C3)}$$

At a median redshift of 3.5 and a distance of 30 kpc, $\Gamma_{\rm obs} \sim 3.5 \times 10^{51}$ photon s^{-1} from which we obtain a Lyman-continuum escape fraction of $f_{\rm esc}^{\rm ISM} \sim 2 \times 10^{-2}$.

This paper has been typeset from a TEX/LATEX file prepared by the author.